Journal of Materials Chemistry C

ROYAL SOCIETY OF CHEMISTRY

PAPER

View Article Online
View Journal

Cite this: DOI: 10.1039/d6tc00832a

Green deep-eutectic synthesis of multinary quantum dots for luminescent polymeric composites and LED applications

Lorenzo Branzi, * Sean Freeman, Lucy Fitzimmons, Conor Burke and Yurii K. Gun'ko *

Received 16th March 2026,
Accepted 12th April 2026

DOI: 10.1039/d6tc00832a

rsc.li/materials-c

The production of a range of multinary quantum dots (QDs), including both ternary phase silver indium sulfide (AIS) and copper indium sulfide (CIS), and their quaternary alloys with zinc sulfide (ZAIS and ZCIS), using a L-menthol and lauric acid deep eutectic solvent (DES) was investigated. This novel synthetic approach relies on the hydrophobic nature of the L-menthol–lauric acid DES to combine the typical reaction environment of hot-injection processes, commonly used for the production of high-quality QDs, with the highly desirable qualities of deep eutectics as green solvents. The deposition of a zinc sulfide shell was also investigated, achieving an improvement of the photoluminescence quantum yield up to 65%. Moreover, the incorporation of multinary QDs produced in the L-menthol–lauric acid DES into polymethyl methacrylate (PMMA) matrices was investigated, yielding both bulk slabs and colour-converting layers for white and monochromatic LEDs. These studies clearly demonstrate the feasibility and advantages of DES-based synthesis for the production of high-quality multinary QDs and their incorporation into luminescent polymeric composites with strong potential for photonic and energy applications.

Introduction

Deep eutectic solvents (DESs) are a family of ionic liquid analogues formed by the hydrogen bond-mediated association of a hydrogen bond acceptor (HBA) and a hydrogen bond donor (HBD), resulting in a eutectic mixture with a significant reduction in the melting point with respect to those of the pure components.[1] DESs are rapidly emerging as promising green alternatives to conventional solvents in terms of biocompatibility, biodegradability, toxicity and availability.[2,3] For these reasons, the development of novel DESs and the investigation of their application in a broad range of processes such as catalysis,[4,5] electrodeposition[6,7] and many others[1,8] have been actively pursued over the last few years. Recently, particular attention has been paid to the synthesis of inorganic nanomaterials using DESs; however, this promising field still remains largely unexplored.[9]

I–III–VI ternary quantum dots and their quaternary zinc alloyed I–II–III–VI phases are a promising class of nanomaterials with visible to near infrared emission. Due to their unique optical properties and composition-dependent tunability, multinary QDs are rapidly becoming popular low-toxicity alternatives to binary II–VI QDs.[10] For these reasons, multinary QDs have been widely investigated in photonics,[10] energy[11] and biomedical applications[12] as well as recent studies have reported efficient hot-electron photocatalysis[13] and tunable chirality.[14,15] In particular, the intrinsic broad photoluminescence and large Stokes shift characteristics of the photoluminescence of multinary QDs make them promising candidates for applications as luminescent active materials in luminescent solar concentrators (LSCs)[16,17] and as downconverter phosphors in colour conversion layers used for white light-emitting diodes (LEDs).[10,18] Despite their promising optical properties and the wide range of technologically relevant applications, synthetic strategies for the production of multinary QDs in DESs have not been reported to date.

In this work, we developed a new robust synthetic procedure using a L-menthol–lauric acid DES for the production of a broad family of luminescent multinary QDs. Our investigation covers ternary I–III–VI compounds such as silver indium sulfide (AIS), copper indium sulfide (CIS) and their quaternary I–II–III–VI phases, including silver indium zinc sulfide (ZAIS) and copper indium zinc sulfide (ZCIS). Hydrophobic DESs represent a relatively novel class of green solvents after the first report in 2015[19] and are becoming rapidly popular, unlocking a wide range of novel applications,[20] among which is their use as solvents for the synthesis of inorganic nanomaterials.[21] The hydrophobic nature of the L-menthol–lauric acid DES mimics the reaction environment typical of hot-injection processes

School of Chemistry, Trinity College Dublin, Dublin, Ireland.
E-mail: branzil@tcd.ie, igounko@tcd.ie

commonly used for the production of high-quality QDs. Moreover, L-menthol and lauric acid are inexpensive natural products characterised by high biocompatibility and natural abundance.[22–24] In particular, L-menthol is produced *via* biosynthesis in plants of *Mentha* species and it is manufactured on a large scale (likely exceeding 700 metric tons per year) for application in industries like oral health care products, the food industry, cosmetics and pharma.[22,23,25] On the other hand, lauric acid is the main component of coconut and palm oil, and vegetable oils and fatty acids are some of the most suitable resources for the development of sustainable processes.[24] To further improve the optical properties of the multinary QDs produced using DES, a one-pot process for the deposition of a ZnS layer and the production of multinary core–shell QDs using the L-menthol–lauric acid DES has been successfully developed, achieving a substantial increase in the photoluminescence quantum yield to values as high as 65%. The hydrophobic nature of the multinary QDs produced *via* this strategy guarantees high compatibility with polymeric matrices like polymethyl methacrylate (PMMA) without any surface modification. Thus, the production of luminescent QD–PMMA bulk nanocomposites *via in situ* radical polymerisation, as well as the fabrication of colour converting layers for application in white and monochromatic LEDs, was investigated.

Results and discussion

A family of luminescent multinary QDs composed of silver, indium, copper and zinc was produced in L-menthol–lauric acid DES using a hot-injection synthesis approach (Fig. 1a). These mixtures are liquid at around 20 °C in agreement with detailed characterisation of the phase behaviour of DES formed by terpenes and monocarboxylic acids reported by Martins and

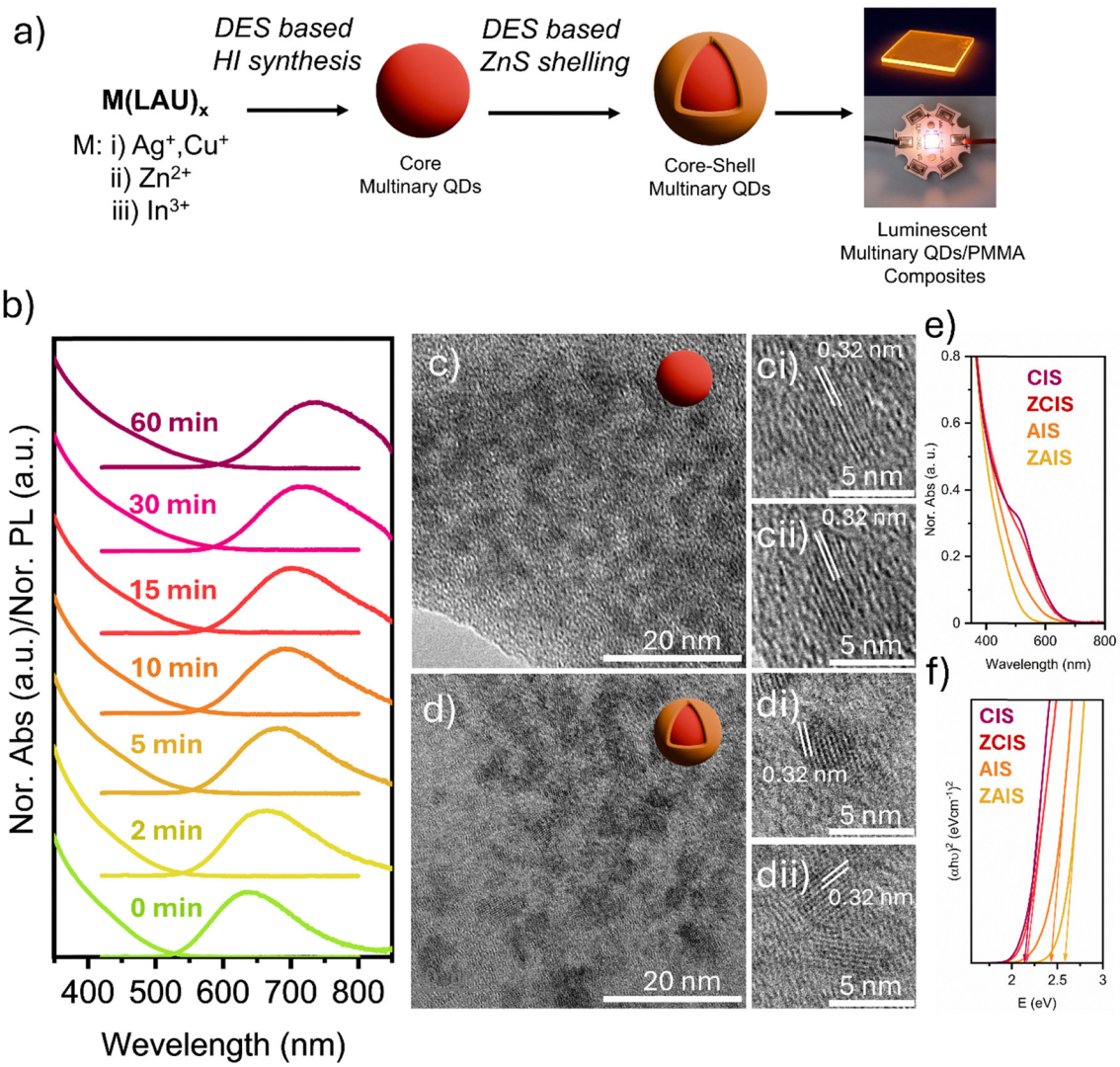

Fig. 1 (a) Scheme of the material production workflow from molecular laurate to luminescent multinary QD–PMMA composites. (b) UV/vis and PL spectra of the AIS QD reaction mixture collected at different growth times at 120 °C. TEM and HR-TEM images of AIS (c), (ci) and (cii) and AIS/ZnS (d), (di) and (dii) QDs. UV/vis spectra (e) and Tauc plots (f) of multinary QDs produced in L-menthol–lauric acid DES.

coworkers.[26] Characterisation details of the L-menthol and lauric acid DES by NMR and FTIR spectroscopy are available in the SI (Fig. S1–S10). In particular, FTIR spectroscopy (Fig. S1) showed a single ν_{OH} at 3400 cm^{-1} for the mixture, higher than those of both the single components. This observation, along with the shift of the ν_{CO} of the lauric acid from 1693 to 1710 cm^{-1}, highlights the formation of the hydrogen network characteristic of the DES.[27] The epitaxial growth of a ZnS shell layer was achieved in a one-pot process by a slow addition of the ZnS precursors, dissolved in the L-menthol–lauric acid DES, to the reaction mixture. Due to the hydrophobic nature of the multinary QDs produced in the L-menthol–lauric acid DES, the nanocrystals can be easily incorporated into PMMA polymer matrices for the production of luminescent composites.

The mixture of L-menthol and lauric acid with a 2 : 1 molar ratio forms a DES which is liquid at room temperature (Fig. S11a and b) and mimics the hydrophobic environment of the high boiling point solvents conventionally used for QD synthesis *via* the hot-injection process.[21,26,27] The use of metal laurate precursors for silver, indium, and zinc enables high solubility of all the different cationic components in the L-menthol–lauric acid DES, allowing for homogeneous solutions even at low temperatures. This was found to be particularly relevant, since a low injection temperature (40 °C) was identified as ideal for the production of QDs with superior optical properties (see later). The injection of the sulfur precursor solution into the metal cation solution in DES induces a rapid particle nucleation, and the nanocrystals' growth can be promoted by further heating at a higher temperature. Fig. 1b shows the typical absorption and photoluminescence spectra of the AIS QD reaction mixture collected at different reaction times. The emission maximum shifts from 636 nm, observed for QDs collected immediately after injection, to around 732 nm after 60 minutes of growth at 120 °C, in agreement with the red-shift of the absorption profile along with an increase in PL intensity (Fig. S11c and d). The QDs' photoluminescence is dramatically affected by the reaction conditions; in particular, injection at 40 °C and a successive heating at 120 °C have been identified as ideal conditions for the synthesis of AIS QDs. Using a higher temperature for the injection step produces QDs with lower PL intensity and a broader emission profile (Fig. S11e), suggesting a poor homogeneity in the QD sample produced at higher temperatures.

TEM images of AIS QDs reveal the presence of nanocrystals with an average size of approximately 2.8 ± 0.9 nm (Fig. 1c and Fig. S12a), while after the deposition of the ZnS shell layer, an increase in the nanocrystal size to 3.5 ± 1.2 nm (Fig. 1d and Fig. S12b) was observed. HR-TEM images reveal diffraction fringes with a spacing of 0.32 nm, corresponding to the (112) planes of the chalcopyrite lattice (*I*-42*d*). Changing the composition of the cation mixture enabled the production of different multinary QDs; in this way, ternary AIS and CIS, as well as their quaternary counterparts with zinc sulfide, ZAIS and ZCIS, QDs were produced using L-menthol–lauric acid DES. The UV/vis absorption of the different multinary QDs is shown in Fig. 1e, and the optical band-gaps were estimated using the Tauc plot method (Fig. 1f), giving band gap values of around 2.14 eV, 2.16 eV, 2.43 eV and 2.58 eV for CIS, ZCIS, AIS and ZAIS QDs, respectively. The increase of the optical band-gap with the incorporation of zinc in the QD cores is consistent with the formation of $AgInS_2$ and $CuInS_2$ alloys with ZnS, forming the respective quaternary systems (Fig. S13).[28]

The PL properties of the multinary QDs produced in L-menthol–lauric acid DES reflect the variations in their chemical composition. PL and PLE spectra of multinary QD cores are shown in Fig. 2ai. Emission at 658 and 595 nm was observed for AIS and ZAIS QDs, while CIS and ZCIS showed emission at 705 and 690 nm, respectively. All systems displayed a broad excitation range that corresponds to the band-gap of the different nanocrystal compositions, as well as the typical emission profile of multinary QDs, characterised by large Stokes shifts and broad emission peaks; these features are associated with the presence of intragap states involved in the radiative recombination mechanism.[29–33] Further details on the optical properties of multinary QDs produced in the L-menthol–lauric acid DES are presented in Table S1. The deposition of the ZnS shell using the L-menthol–lauric acid DES-based approach improves the PLQY (Table S1) for all the multinary QDs. In particular, the PLQY of ZAIS QDs increased from 18% to 65% with the deposition of the ZnS shell (Fig. S14). This enhancement is attributed to the passivation of surface defects such as dangling bonds with a layer of a larger bandgap semiconductor, suppressing non-radiative recombination pathways.[34] Moreover, the ZnS shell deposition causes a further blue shift of the emission profiles, as shown in Fig. 2aii, which can be associated with a partial diffusion of Zn^{2+} ions in the QD core.[35] The incorporation of Zn^{2+} into the QD core *via* the direct synthesis of quaternary I–II–III–VI systems or *via* diffusion is expected to mitigate the effect of cationic disorder and further improve optical properties.[36] The effect of the ZnS shell deposition on the exciton recombination mechanism was further supported by the analysis of the PL lifetime observed at the PL maximum. All the I–III–VI multinary QDs produced showed photoluminescence decays on the order of 100–500 ns (Fig. S15), and these are typical values for I–III–VI QDs where the exciton recombination mechanism is mediated by intragap donor–acceptor states. An increase of the average lifetime of around 90 ns was observed for ZAIS, CIS and ZCIS QDs after the passivation process with ZnS (Table S2), supporting the suppression of non-radiative recombination processes with the deposition of an inorganic shell. In contrast, AIS QDs did not show any appreciable variation in the PL lifetime; however, this system is characterised by the longer decay time ($\langle\tau\rangle$ of around 480 ns) and variation in the average lifetime may not as evident as that of the other multinary QDs discussed here. Moreover, the observed lifetime of multinary QDs is wavelength dependent due to the complex mechanism involved in the exciton recombination and this could further complicate this analysis.[37] The effect of the ZnS shell deposition on QDs' optical properties was demonstrated in the photoluminescence thermal stability. The PL of ZAIS QDs decreases to 58% when the nanocrystals are heated at 60 °C (Fig. S16a and c), while 85% of the PL is

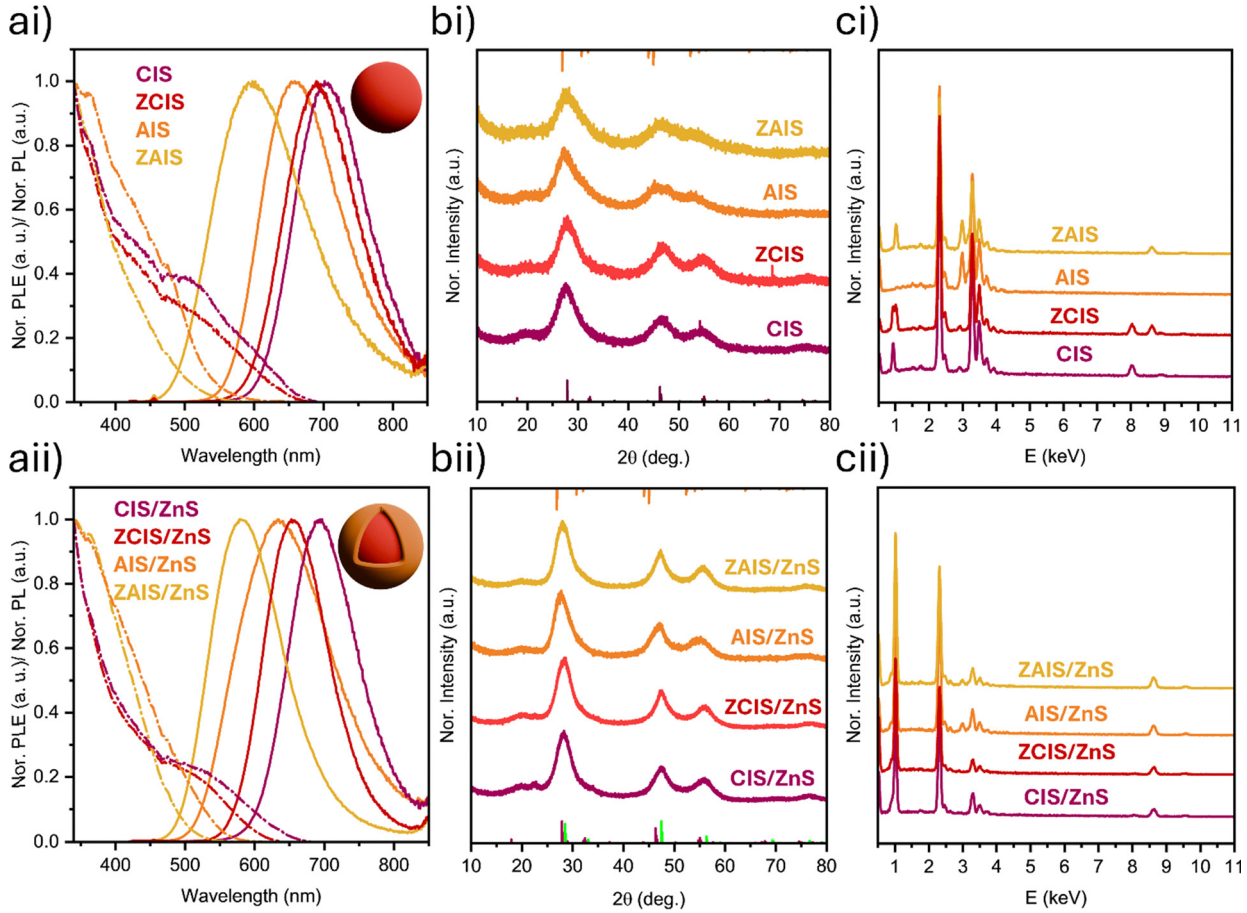

Fig. 2 PL and PLE spectra (a), XRD patterns (b), and EDS spectra (c) of multinary core (i) and core/shell (ii) QDs produced using L-menthol–lauric acid DES. Reference patterns used for XRD: $AgInS_2$ $I\bar{4}2d$ COD 1509400 (orange), $CuInS_2$ $I\bar{4}2d$ ICSD 66865 (wine) and ZnS $F\bar{4}3m$ COD 1100043 (green).

preserved for the ZAIS/ZnS QDs (Fig. S16b and c). This observation further supports the critical role of the ZnS shell deposition in device applications such as LEDs.

XRD analysis revealed diffraction patterns that correspond to the tetragonal chalcopyrite phase, $I\bar{4}2d$ space group (Fig. 2bi) for all multinary core QD systems, in agreement with the TEM observations. The effect of Zn incorporation on the quaternary QDs is highlighted by the shift of all the peaks to slightly larger angles due to the smaller ionic radius of Zn^{2+} compared to that of In^{3+}.[38] In particular, the (112) peak is located at 27.2° for AIS QDs and 27.9° for ZAIS QDs. Similarly, the (204) and (312) peaks are shifted from 46.1° to 46.8° and from 53.0° to 53.9° (Fig. S17a and c), respectively. This evidence suggests a contraction of the *d*-spacing from 3.28, 1.97 and 1.73 Å observed for AIS QDs to 3.20, 1.94 and 1.70 Å in the case of ZAIS QDs. After the deposition of the ZnS layer, the diffraction patterns are dominated by the contribution of the sphalerite ZnS phase, space group $F\bar{4}3m$ (Fig. 2bii and Fig. S17b), as supported by Rietveld refinement (Fig. S18). The shelling step introduced an additional shift of all the diffraction peaks toward larger angles in comparison with the pattern of the core QDs (Fig. S19),[34,39] along with a reduction of the peak broadening that can be associated with an increase in the crystalline size. Scherrer analysis of the broadening of the (112) peak gave crystalline sizes of 2.0 and 2.7 nm for ZAIS and ZAIS/ZnS QDs, respectively, further supporting the TEM evidence.

Energy dispersive X-ray spectroscopy (EDS) analysis of the multinary core QDs (Fig. 2ci) was performed to investigate the nanocrystals' chemical composition. For the purpose of this work, we targeted the production of indium-rich QDs, since these systems are known for their superior optical properties associated with the formation of intrinsic defects.[40,41] The EDS spectra of AIS QDs confirmed an Ag : In ratio of around 1 : 3.5, close to the composition used in the reaction mixture of 1 : 4. The quaternary ZAIS QDs showed a lower indium content with a ratio of 1 : 1 : 2.5 for Ag : Zn : In, respectively, suggesting that Zn^{2+} mostly replaced In^{3+} in the core QD structure (Fig. S20a). Similar observations were made for the copper-based QDs with the Cu : In ratio of 1 : 3.1 for the ternary CIS QDs, while a Cu : Zn : In ratio of 1 : 1.1 : 2.5 was observed for the quaternary ZCIS QDs (Fig. S20a). The deposition of ZnS significantly increased the zinc contribution for all the QDs (Fig. 2cii), and a ratio of around 1 : 2.8 was observed between the sum of the contributions from the monovalent and trivalent cations and Zn (Fig. S20b) for AIS/ZnS QDs and 1 : 2.6 for CIS/ZnS QDs.

To evaluate the potential applications of multinary QDs produced in the L-menthol–lauric acid DES, the production of luminescent multinary QD–PMMA nanocomposites was

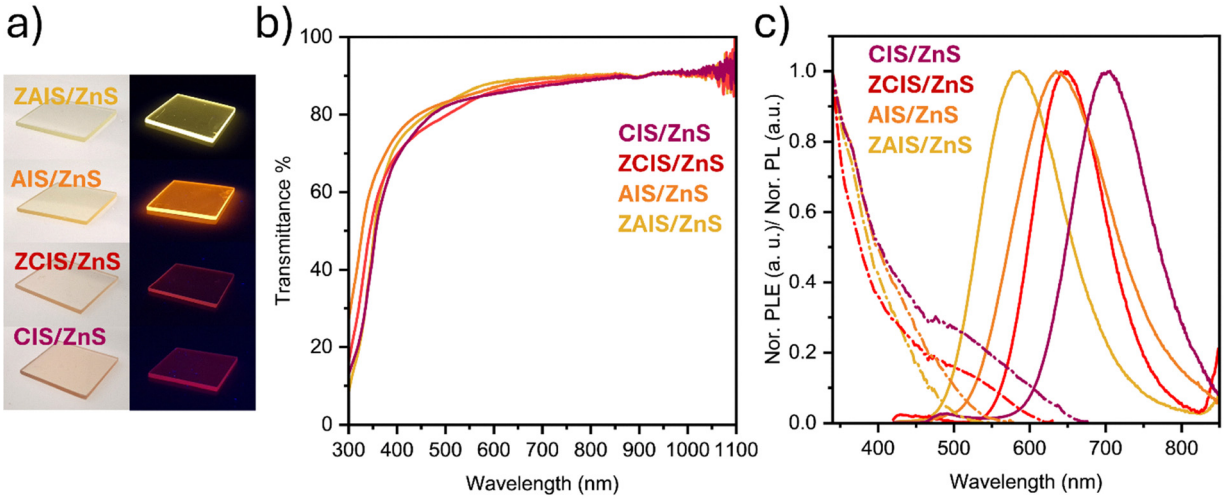

Fig. 3 (a) Photograph of the PMMA core–shell multinary QDs under ambient and UV illumination conditions, with a size of 2.5 × 2.5 × 0.2 cm. Transmission (b) and PLE/PL spectra (c) of core/shell PMMA core–shell multinary QD nanocomposites.

investigated. PMMA is an ideal candidate for the production of luminescent QD–polymer nanocomposites for application in photonics, due to its high optical transparency, stability and mechanical properties.[42] For this purpose, multinary core–shell QDs were used, due to their superior optical properties, for the preparation of QD–PMMA bulk slabs *via in situ* radical polymerisation of methacrylic acid, as well as the production of QD–PMMA coating layers starting from PMMA solution in toluene.

For the production of multinary QD–PMMA bulk slabs, a two-step process was employed where the methyl methacrylate monomer was polymerised to a syrup in the first step, before the addition of the multinary QD solution and transfer into a sheet reactor mould to complete the polymerisation. Fig. 3 shows the optical characterisation of multinary QD–PMMA composite slabs (2.5 × 2.5 × 0.2 cm) produced using a QD loading of around 0.025 wt%. The QD–PMMA composites obtained by this procedure were highly transparent and homogeneous, preserving the optical properties of the multinary QDs used (Fig. 3a). The transmission spectra (Fig. 3b) show a maximum of transmittance of around 90% (at wavelengths higher than 700 nm), indicating a low degree of scattering caused by QD aggregation in the polymeric composite. The loss of around 10% in transmission is expected due to reflections from the two surfaces of the polymeric slab, while the absorption at shorter wavelengths reflects the chemical composition of the multinary QD used.[43,44] More importantly, the photoluminescence properties of the multinary QDs (PL and PLE) are preserved in the PMMA nanocomposites (Fig. 3c), with emission maxima centred at 585 nm, 635 nm, 650 nm and 702 nm for ZAIS/ZnS, AIS/ZnS, ZCIS/ZnS and CIS/ZnS QDs, respectively. These types of composites are of great interest for potential application in LSC devices, where the large Stokes shift of multinary QDs ensures minimal energy losses due to reabsorption processes.[16,17]

The potential application of multinary QDs produced in L-menthol–lauric acid DES as colour converting phosphors for LEDs was investigated by preparing different QD–PMMA mixtures using a QD loading concentration of around 2.5 wt% on top of an LED chip to produce colour conversion layers with different optical properties. QDs have recently become a promising alternative to solid-state phosphors to produce white LEDs, especially multinary QDs, due to their intrinsic broad emission spectra.[10,18] In particular, coating a 475 nm blue LED (forward voltage and current applied to the LED chip: 3.0 V and 80 to 140 mA, respectively) with ZAIS/ZnS (Fig. 4a) resulted in white light with CIE coordinates of $X = 0.423$ and $Y = 0.3911$ (Fig. 4c), a colour rendering index (CRI) of 77 and a correlated colour temperature (CCT) of 3100 K corresponding to warm white light. Similarly, AIS/ZnS QDs (Fig. 4b) produced warm white light with a larger contribution from the red spectral range, with CIE coordinates $X = 0.503$ and $Y = 0.4038$ (Fig. 4c), a CRI of 80, and a CCT of around 2100 K. Details on the effect of varying the current applied to the LED chip are shown in Fig. S21. A comparison with commercial white LEDs (Fig. S22) revealed that colour conversion layers produced using multinary QDs prepared in L-menthol–lauric acid DES have comparable CIE coordinates with commercial systems.

However, the colour rendering properties of multinary QD-based LEDs are still limited; commercial white LEDs showed a CRI of 97 and 92, mainly due to the stronger luminescence contribution in the green spectral range of their phosphor materials. The application of these QDs in the production of colour conversion layers for the production of monochromatic LEDs was investigated as well. In particular, yellow and red emissions were produced by coating a 400 nm LED chip with ZAIS/ZnS (Fig. 4d) and ZCIS/ZnS (Fig. 4e) QDs, respectively. The colour conversion layers produced light with CIE coordinates $X = 0.564$ and $Y = 0.432$ for ZAIS/ZnS QDs, while light with CIE coordinates $X = 0.649$ and $Y = 0.343$ was obtained using ZCIS/ZnS (Fig. 4f).

Conclusions

Thus, a variety of luminescent multinary QDs were successfully synthesised using the L-menthol–lauric acid DES *via* a hot-injection synthesis. These observations open possibilities for

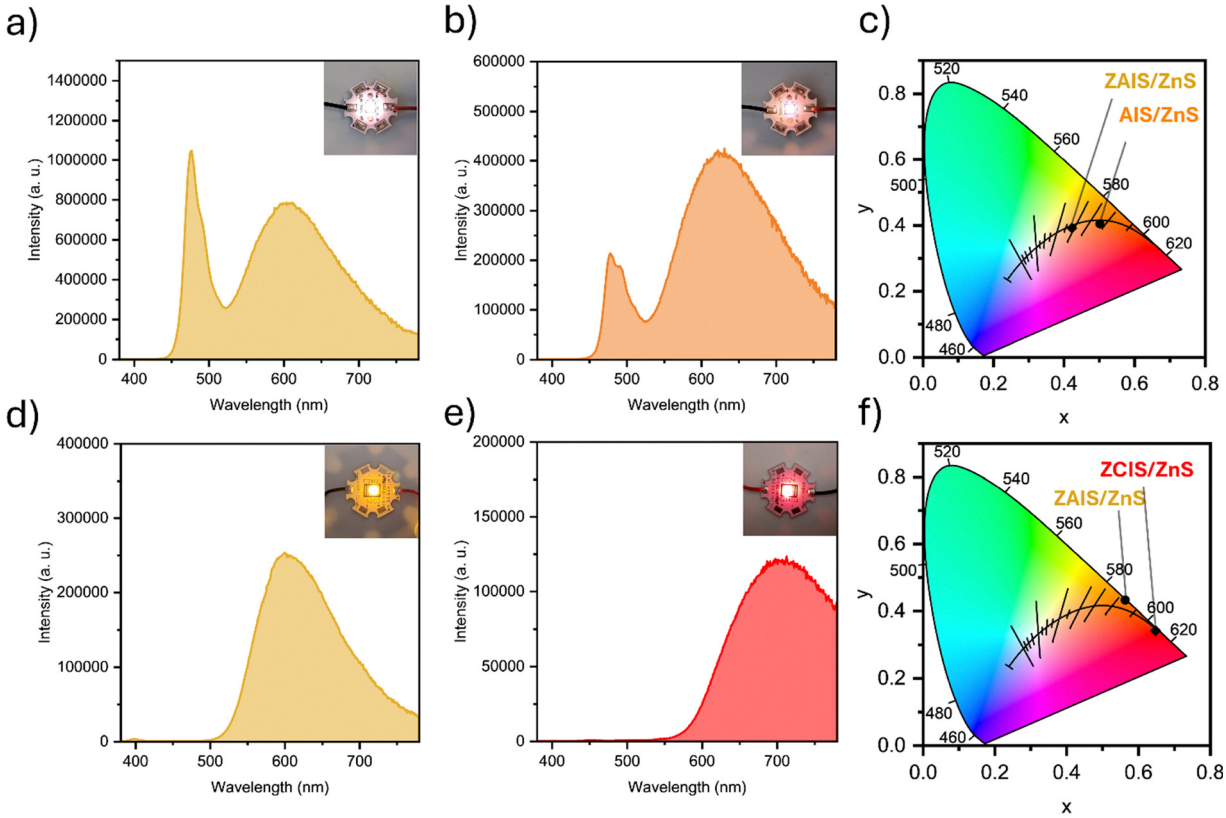

Fig. 4 Luminescence spectra of white LEDs produced using ZAIS/ZnS (a) and AIS/ZnS (b) multinary QDs and relative CIE chromaticity coordinate diagram (c). Luminescence spectra of monochromatic LEDs produced using ZAIS/ZnS (d) and ZCIS/ZnS (e) multinary QDs and the relative CIE chromaticity coordinate diagram (f).

the development of novel processes to produce multinary QDs that rely on sustainable products naturally biosynthesised in plants. These may lead to attractive alternatives to conventional hot-injection approaches that heavily rely on high-boiling point solvents like 1-oleylamine and 1-octadecene which require a more hazardous production.[45,46] In particular, issues related to the purity and cost of 1-oleylamine have been previously identified as critical limitations for the industrial production of nanomaterials.[47,48] Thus, the development of alternative sustainable syntheses that limit the use of such solvents is critical for the scale-up of nanomaterial production. Our synthetic approach enabled the production of a broad range of multinary luminescent QDs, including ternary silver indium sulfide and copper indium sulfide QDs, as well as quaternary silver zinc indium sulfide and copper zinc indium sulfide QDs. Moreover, it was possible to obtain the respective core–shell QD systems *via* a DES-based deposition of zinc sulfide, resulting in photoluminescence quantum yields of up to 65%. Due to the hydrophobic nature of the QDs produced in the L-menthol–lauric acid DES, the nanocrystals can be easily incorporated into PMMA polymer matrices. The production of luminescent QD–PMMA composites was developed both *via* direct radical polymerisation and by using PMMA solution for the production of bulk slabs and colour converting layers, respectively. Finally, the potential application of luminescent multinary QD–PMMA nanocomposites as LED colour converting layers was investigated for the production of white as well as monochromatic LEDs. Overall, this work presents a new synthetic strategy that combines the advantages of heavy metal-free multinary QDs with the low environmental impact of a DES, enabling the sustainable production of luminescent multinary nanocrystals for photonic and energy applications.

Experimental

Materials

Indium acetate (99.99%) and L-menthol (99%) were purchased from Thermo Scientific. Copper sulphate pentahydrate (>99%) was purchased from Acros Organics. Silver nitrate (≥99.8%), zinc nitrate hexahydrate (≥99%), sulphur (≥99%), sodium hydroxide (≥98%), lauric acid (98%), lauroyl peroxide (97%), oleylamine (70%), 1-dodecanethiol (98%), and methyl methacrylate (99%) were purchased from Sigma-Aldrich. Polymethyl methacrylate with MW ≈ 120 000 was purchased from Aldrich. The LED chips ILH-XO01-S390-SC211-WIR200 (400 nm LED), ILH-OW01-BLUE-SC211-WIR200 (475 nm), and ILH-OT01-HW90-SC221-WIR200-1 hot white (2700 K) and white (5000 K) were purchased from Intelligent LED Solutions ILS.

Characterisation

Infrared spectra were collected using a PerkinElmer Spectrum 100 FTIR spectrophotometer equipped with ATR. NMR data

were collected with a Bruker Avance III 400 MHz spectrometer (proton frequency of 400.23 MHz) equipped with a 5.0 mm BBOF probe. UV-vis absorption spectra of colloidal solution of QDs in toluene were recorded using an Agilent Cary 60 spectrophotometer. Photoluminescence and photoluminescence excitation spectra were recorded with a Horiba FluoroMax-4. Photoluminescence quantum yields were measured using a rhodamine 6G solution in water as the photoluminescence standard with an excitation wavelength of 485 nm and an absorbance of 0.025. Emission spectra of both the standard and samples were collected in the range of 500 to 850 nm. The PLQY values were calculated according to eqn (1),[49,50]

$$\Phi_{QD} = \Phi_{st} F_{QD} f_{st} n_{QD}^2 / F_{st} f_{QD} n_{st}^2 \quad (1)$$

where Φ is the PLQY, F is the integrated intensity of the emission peak, n is the refractive index of the solvent and f is the absorption coefficient estimated according to eqn (2), where A corresponds to the absorbance of the QD sample, QD, and standard, st, respectively,

$$f_{QD,st} = 1 - 10^{-A_{QD,st}}. \quad (2)$$

Photoluminescence lifetime measurements were collected using a Horiba Fluorolog with NanoLed-370 (372 nm, pulse duration 1.1 nm) as an excitation source.

TEM images were collected using a JEOL 2100 microscope operating at 200 kV. EDS spectra were collected on a ZEISS Ultra Plus SEM equipped with a Bruker XFlash 7 7100 EDS detector with a 100 m^2 window using a 15 kV electron beam. For each type of multinary QDs, EDS spectra were acquired over an area of 100 × 100 μm and the chemical composition was calculated as the average of three measurements. XRD patterns were collected using a Bruker D2 Phaser X-ray Powder Diffractometer working with the Cu Kα radiation source. FullProf software was used for the Rietveld refinement. LED colour converting layer characterisation was performed, powering the LED source at 100 mA and collecting the emission spectra using an integration sphere.

Syntheses

Synthesis of metal laurate precursors. A 0.25 M sodium laurate solution was produced by dissolving lauric acid (0.5 mol) and sodium hydroxide (0.5 mol) in 500 mL of deionised water in a water bath at 40 °C. When the lauric acid was completely solubilised, the solution was removed from the water bath and stored at room temperature (the sodium laurate solution slowly freezes at room temperature and must be warmed up to obtain a homogeneous liquid before use). 1 mmol of metal salt ($AgNO_3$, $Cu(SO_4)_2$, $In(OAc)_3$ or $Zn(NO_3)_2x6H_2O$) was solubilised in 20 mL of deionised water in a water bath at 40 °C. A stoichiometric amount of sodium laurate was added under constant stirring, causing the precipitation of the metal laurate. Then, the product was isolated by filtration or sedimented *via* centrifugation and washed three times with 20 mL of deionised water and once with 20 mL of methanol before being dried overnight under vacuum at room temperature.

Sulfide precursor solution. Sulfur (70 mg) was solubilised in oleylamine (1 mL) and 1-dodecanthiol (0.5 mL).

ZnS precursor solution. Zinc laurate (464 mg, 1 mmol) was dispersed in menthol (2 g, 0.0128 mol) and lauric acid (1.3 g, 0.0065 mol). Then, the sulfide precursor solution (400 μL) was added, producing a final volume of around 4 mL.

Synthesis of core multinary QDs in DES. In the general synthesis of AIS QDs, menthol (1.0 g, 6.4 mmol), lauric acid (650 mg, 3.2 mmol), silver laurate (20 mg, 0.065 mmol) and indium laurate (185 mg, 0.260 mmol) were mixed in a Schlenk tube. 1-Dodecanthiol (125 μL) was added, and the mixture was heated up to 80 °C under vacuum for 15 min before switching the atmosphere to nitrogen. Then, the solution was transferred to a water bath at 40 °C and allowed to equilibrate for 5 min before injecting the sulfide precursor solution (300 μL). After 5 min, the tube was moved to an oil bath at 120 °C, and the nanocrystals were allowed to grow for 30 min. Then, the reaction mixture was cooled in a room temperature water bath, and 15 mL of toluene was added. The product was collected by centrifugation (9000 rpm, 1 min) after the addition of around 5 mL of ethanol and washed two more times before being stored in a solution of 25 mM 1-DDT and 50 mM OLA in toluene for further use. For the production of CIS and ZCIS, copper laurate (30 mg, 0.065 mmol) was used instead of silver laurate. Instead, in the case of the quaternary QDs, a mixture of silver laurate and zinc laurate (40 mg, 0.086 mmol) or a mixture of copper laurate and zinc laurate (40 mg, 0.086 mmol) was used for the production of ZAIS and ZCIS, respectively.

Synthesis of core–shell multinary QDs in DES. Directly after heating the reaction mixture for the production of the core multinary QDs at 120 °C for 30 min, the reaction mixture was transferred to an oil bath at 180 °C. The ZnS precursor solution was injected using a syringe pump at a rate of 4 mL h^{-1}. When the injection was completed, the reaction mixture was cooled down in a room temperature water bath, and toluene (15 mL) was added. The product was isolated by centrifugation (9000 rpm, 1 min) after the addition of around 5 mL of ethanol and washed two more times before being stored in a solution of 25 mM 1-DDT and 50 mM OLA in toluene for further use.

Production of bulk luminescent QD–PMMA nanocomposites. Lauroyl peroxide (30 mg) was solubilised in methyl methacrylate (6 mL) under nitrogen flux. The solution was heated at 70 °C for 30 min before adding the QD stock solution (150 μL). Then, the reaction mixture was transferred into a sheet reactor made of two panes of glass with a PVC gasket. The reactor was placed in a water bath at 55 °C for around 4 h to allow the polymer to fully cure. Once fully hardened, the PMMA slab was removed from the reactor and cut into 2.5 × 2.5 cm samples and the edges were sanded.

Production of LED colour converting layers. Ethanol (0.5 mL) was added to the QD solution (200 μL) and the QDs were isolated by centrifugation (9000 rpm, 1 min). The pellet was dispersed in a solution of PMMA (20%$_{w/v}$ in toluene). The mixture (50 μL, QD concentration around 2.5 wt%) was then deposited on top of the LED chip and allowed to dry at room temperature.

Author contributions

L. Branzi and Y. K. Gun'ko conceived the project. The investigations were conducted by L. Branzi, S. Freeman, L. Fitzimmons,

and C. Burke. Funding, resources, and supervision were provided by Y. K. Gun'ko. Writing and data visualization were carried out by L. Branzi.

Conflicts of interest

There are no conflicts to declare.

Data availability

Data are available upon request from the authors.

Supplementary information (SI): FTIR, UV-Vis, PL and NMR spectra, photoluminescence decay curves, XRD patterns, EDS analysis, additional TEM and HR-TEM images of QDs and luminescence spectra of LEDs. See DOI: https://doi.org/10.1039/d6tc00832a.

Acknowledgements

The authors gratefully acknowledge Research Ireland (projects: SFI-20/FFP-A/8904 and 21/RC/10307_P2) for their financial support. The microscopy characterisation and analysis were performed at the TCD Advanced Microscopy Laboratory (AML).

Notes and references

1 Q. Zhang, K. De Oliveira Vigier, S. Royer and F. Jérôme, *Chem. Soc. Rev.*, 2012, **41**, 7108–7146.
2 B.-Y. Zhao, P. Xu, F.-X. Yang, H. Wu, M.-H. Zong and W.-Y. Lou, *ACS Sustainable Chem. Eng.*, 2015, **3**, 2746–2755.
3 Y. Huang, F. Feng, J. Jiang, Y. Qiao, T. Wu, J. Voglmeir and Z.-G. Chen, *Food Chem.*, 2017, **221**, 1400–1405.
4 L. Xu, J. Yin, J. He, H. Li, L. Zhu, H. Ning, K. Jie, W. Zhu, H. Li, S. Dai and W. Jiang, *Adv. Mater.*, 2024, **36**, 2313853.
5 X. Yang, Q. Zou, T. Zhao, P. Chen, Z. Liu, F. Liu and Q. Lin, *ACS Sustainable Chem. Eng.*, 2021, **9**, 10437–10443.
6 S. Liu, Y. Cao, L. Yang, Y. Li, J. Li, B. Xin, G. Feng, H. Wang and C. Wang, *Small*, 2025, **21**, 2500641.
7 M. Manolova, R. Böck, I. Scharf, T. Mehner and T. Lampke, *J. Alloys Compd.*, 2021, **855**, 157462.
8 E. L. Smith, A. P. Abbott and K. S. Ryder, *Chem. Rev.*, 2014, **114**, 11060–11082.
9 T. Zhang, T. Doert, H. Wang, S. Zhang and M. Ruck, *Angew. Chem., Int. Ed.*, 2021, **60**, 22148–22165.
10 L. Yang, S. Zhang, B. Xu, J. Jiang, B. Cai, X. Lv, Y. Zou, Z. Fan, H. Yang and H. Zeng, *Nano Lett.*, 2023, **23**, 2443–2453.
11 M. Sandroni, R. Gueret, K. D. Wegner, P. Reiss, J. Fortage, D. Aldakov and M.-N. Collomb, *Energy Environ. Sci.*, 2018, **11**, 1752–1761.
12 W. M. Girma, M. Z. Fahmi, A. Permadi, M. A. Abate and J.-Y. Chang, *J. Mater. Chem. B*, 2017, **5**, 6193–6216.
13 J. Feng, K. Fan, Q. Cao, W. Liang, P. Y. Wong, J. Xue, K. T. Chang, K. S. Wong and H. Lu, *Angew. Chem., Int. Ed.*, 2025, **64**, e202508543.
14 L. Branzi, A. Ciotti, A. Kavanagh, E. Feehily, M. García-Melchor and Y. K. Gun'ko, *J. Colloid Interface Sci.*, 2026, **703**, 139246.
15 L. Branzi, F. Purcell-Milton, C. Cressoni, M. Back, E. Cattaruzza, A. Speghini, Y. K. Gun'ko and A. Benedetti, *Nanoscale*, 2022, **14**, 12174–12182.
16 F. Meinardi, H. McDaniel, F. Carulli, A. Colombo, K. A. Velizhanin, N. S. Makarov, R. Simonutti, V. I. Klimov and S. Brovelli, *Nat. Nanotechnol.*, 2015, **10**, 878–885.
17 A. Anand, M. L. Zaffalon, G. Gariano, A. Camellini, M. Gandini, R. Brescia, C. Capitani, F. Bruni, V. Pinchetti, M. Zavelani-Rossi, F. Meinardi, S. A. Crooker and S. Brovelli, *Adv. Funct. Mater.*, 2020, **30**, 1906629.
18 C. C. Lin and R.-S. Liu, *J. Phys. Chem. Lett.*, 2011, **2**, 1268–1277.
19 D. J. G. P. Van Osch, L. F. Zubeir, A. Van Den Bruinhorst, M. A. A. Rocha and M. C. Kroon, *Green Chem.*, 2015, **17**, 4518–4521.
20 C. Florindo, L. C. Branco and I. M. Marrucho, *ChemSusChem*, 2019, **12**, 1549–1559.
21 S. Chatterjee, A. Sen and P. Sen, *Mater. Chem. Front.*, 2023, **7**, 753–764.
22 T. Patel, Y. Ishiuji and G. Yosipovitch, *J. Am. Acad. Dermatol.*, 2007, **57**, 873–878.
23 K. Fahlbusch, F. Hammerschmidt, J. Panten, W. Pickenhagen, D. Schatkowski, K. Bauer, D. Garbe and H. Surburg, *Ullmann's Encyclopedia of Industrial Chemistry*, Wiley-VCH, Wiley, 1st edn, 2003.
24 D. J. Anneken, S. Both, R. Christoph, G. Fieg, U. Steinberner and A. Westfechtel, *Ullmann's Encyclopedia of Industrial Chemistry*, Wiley-VCH, Wiley, 1st edn, 2006.
25 R. B. Croteau, E. M. Davis, K. L. Ringer and M. R. Wildung, *Sci. Nat.*, 2005, **92**, 562.
26 M. A. R. Martins, E. A. Crespo, P. V. A. Pontes, L. P. Silva, M. Bülow, G. J. Maximo, E. A. C. Batista, C. Held, S. P. Pinho and J. A. P. Coutinho, *ACS Sustainable Chem. Eng.*, 2018, **6**, 8836–8846.
27 B. D. Ribeiro, C. Florindo, L. C. Iff, M. A. Z. Coelho and I. M. Marrucho, *ACS Sustainable Chem. Eng.*, 2015, **3**, 2469–2477.
28 T. Kameyama, T. Takahashi, T. Machida, Y. Kamiya, T. Yamamoto, S. Kuwabata and T. Torimoto, *J. Phys. Chem. C*, 2015, **119**, 24740–24749.
29 T. Chevallier, G. Le Blevennec and F. Chandezon, *Nanoscale*, 2016, **8**, 7612–7620.
30 A. S. Fuhr, H. J. Yun, N. S. Makarov, H. Li, H. McDaniel and V. I. Klimov, *ACS Photonics*, 2017, **4**, 2425–2435.
31 A. S. Baimuratov, I. V. Martynenko, A. V. Baranov, A. V. Fedorov, I. D. Rukhlenko and S. Yu Kruchinin, *J. Phys. Chem. C*, 2019, **123**, 16430–16438.
32 Y. Hamanaka, K. Ozawa and T. Kuzuya, *J. Phys. Chem. C*, 2014, **118**, 14562–14568.
33 O. Stroyuk, F. Weigert, A. Raevskaya, F. Spranger, C. Würth, U. Resch-Genger, N. Gaponik and D. R. T. Zahn, *J. Phys. Chem. C*, 2019, **123**, 2632–2641.
34 L. Branzi, J. Liang, G. Dee, A. Kavanagh and Y. K. Gun'ko, *ACS Appl. Mater. Interfaces*, 2024, **16**, 37017–37027.

35 S. P. Hong, H. K. Park, J. H. Oh, H. Yang and Y. R. Do, *J. Mater. Chem.*, 2012, **22**, 18939–18949.
36 M. Yarema, N. Yazdani, O. Yarema, N. Đorđević, W. M. M. Lin, D. Bozyigit, S. Volk, A. Moser, A. Turrini, P. A. Khomyakov, M. Nachtegaal, M. Luisier and V. Wood, *Adv. Mater.*, 2024, **36**, 2406351.
37 Y. Hamanaka, T. Ogawa, M. Tsuzuki and T. Kuzuya, *J. Phys. Chem. C*, 2011, **115**, 1786–1792.
38 M. D. Regulacio, K. Y. Win, S. L. Lo, S.-Y. Zhang, X. Zhang, S. Wang, M.-Y. Han and Y. Zheng, *Nanoscale*, 2013, **5**, 2322–2327.
39 A. Zhang, C. Dong, L. Li, J. Yin, H. Liu, X. Huang and J. Ren, *Sci. Rep.*, 2015, **5**, 15227.
40 M. Uehara, K. Watanabe, Y. Tajiri, H. Nakamura and H. Maeda, *J. Chem. Phys.*, 2008, **129**, 134709.
41 B. Chen, H. Zhong, W. Zhang, Z. Tan, Y. Li, C. Yu, T. Zhai, Y. Bando, S. Yang and B. Zou, *Adv. Funct. Mater.*, 2012, **22**, 2081–2088.
42 M. J. Smith, C. H. Lin, S. Yu and V. V. Tsukruk, *Adv. Opt. Mater.*, 2019, **7**, 1801072.
43 Y. Ma, B. Zhang, M. Gu, S. Huang, X. Liu, B. Liu and C. Ni, *J. Appl. Polym. Sci.*, 2013, **130**, 1548–1553.
44 H. Althues, R. Palkovits, A. Rumplecker, P. Simon, W. Sigle, M. Bredol, U. Kynast and S. Kaskel, *Chem. Mater.*, 2006, **18**, 1068–1072.
45 K. Griesbaum, A. Behr, D. Biedenkapp, H. Voges, D. Garbe, C. Paetz, G. Collin, D. Mayer and H. Höke, *Ullmann's Encyclopedia of Industrial Chemistry*, Wiley-VCH, Wiley, 1st edn, 2000.
46 K. Eller, E. Henkes, R. Rossbacher and H. Höke, *Ullmann's Encyclopedia of Industrial Chemistry*, Wiley-VCH, Wiley, 1st edn, 2000.
47 S. Mourdikoudis and L. M. Liz-Marzán, *Chem. Mater.*, 2013, **25**, 1465–1476.
48 D. Baranov, M. J. Lynch, A. C. Curtis, A. R. Carollo, C. R. Douglass, A. M. Mateo-Tejada and D. M. Jonas, *Chem. Mater.*, 2019, **31**, 1223–1230.
49 A. M. Brouwer, *Pure Appl. Chem.*, 2011, **83**, 2213–2228.
50 U. Resch-Genger and K. Rurack, *Pure Appl. Chem.*, 2013, **85**, 2005–2013.